


Effect of preparation method on alginate wafer properties

Ernest Man¹ | Adeolu Oluwasanmi¹ | Dimitrios A. Lamprou² |
Kirsty Goudie¹ | John Liggat¹ | Clare Hoskins¹ 

¹Department of Pure and Applied Chemistry, University of Strathclyde, Glasgow, UK

²School of Pharmacy, Queen's University Belfast, Belfast, UK

Correspondence

Clare Hoskins, Department of Pure and Applied Chemistry, University of Strathclyde, 99 George Street, Glasgow, G1 1RD, UK.

Email: clare.hoskins@strath.ac.uk

Abstract

The utilization of alginate polymers for wound healing is well explored; however, little attention is paid toward the optimization of the manufacturing process, especially in regards to the final morphological and rheological properties that are imparted to the alginate matrix. This is important as it helps to establish a set of guidelines for the consistent fabrication of mechanically strong polymer wafers, which in the context of manufacturing and production contributes to the reduction in research and development time required. In this study, the order of application with respect to cross-linking and freeze-drying parameters has been investigated, which showed to result in distinct differences in terms of their overall morphology and mechanical strength. The application of freeze-drying before cross-linking results in the uniform distribution of cross-links throughout the alginate wafer, thereby producing a mechanically strong polymer wafer that retains the dehydrated matrices original thickness and architecture. Based on the observed data, freeze-drying prior to cross-linking facilitates the increased permeation and distribution of the cross-linker solution into the polymer matrix, thus resulting in the uniform distribution of ionic cross-links, which is necessary to produce a more mechanically superior polymer matrix.

KEYWORDS

applications, differential scanning calorimetry, drug delivery systems, mechanical properties, rheology

1 | INTRODUCTION

Alginates are one of the most highly utilized polymers in the field of regenerative medicine, with usage in wound healing,^{1,2} drug delivery,^{3–5} and tissue engineering,^{6,7} among many others. The mass usage of alginates derives primarily from its abundance in nature, whereby it can be sustainably sourced from a variety of seaweed species including *Ascophyllum*, *Durvillaea*, *Ecklonia*, *Lessonia*,

Laminaria, and *Macrocystis*, as well as from the bacterial species of *Azotobacter* and *Pseudomonas*.⁸

The standard fabrication method of alginate hydrogels first begin with the solvation of sodium alginate, which produces sodium cations and alginic acid.^{9,10} The molecular structure of alginic acid follows the standard repeating pattern of two linked β -D-mannuronate (*M*) residues coupled to two linked L-gulonate residues (*G*) Figure 1a. When a calcium chloride cross-linker solution

This is an open access article under the terms of the [Creative Commons Attribution](https://creativecommons.org/licenses/by/4.0/) License, which permits use, distribution and reproduction in any medium, provided the original work is properly cited.

© 2022 The Authors. *Journal of Applied Polymer Science* published by Wiley Periodicals LLC.

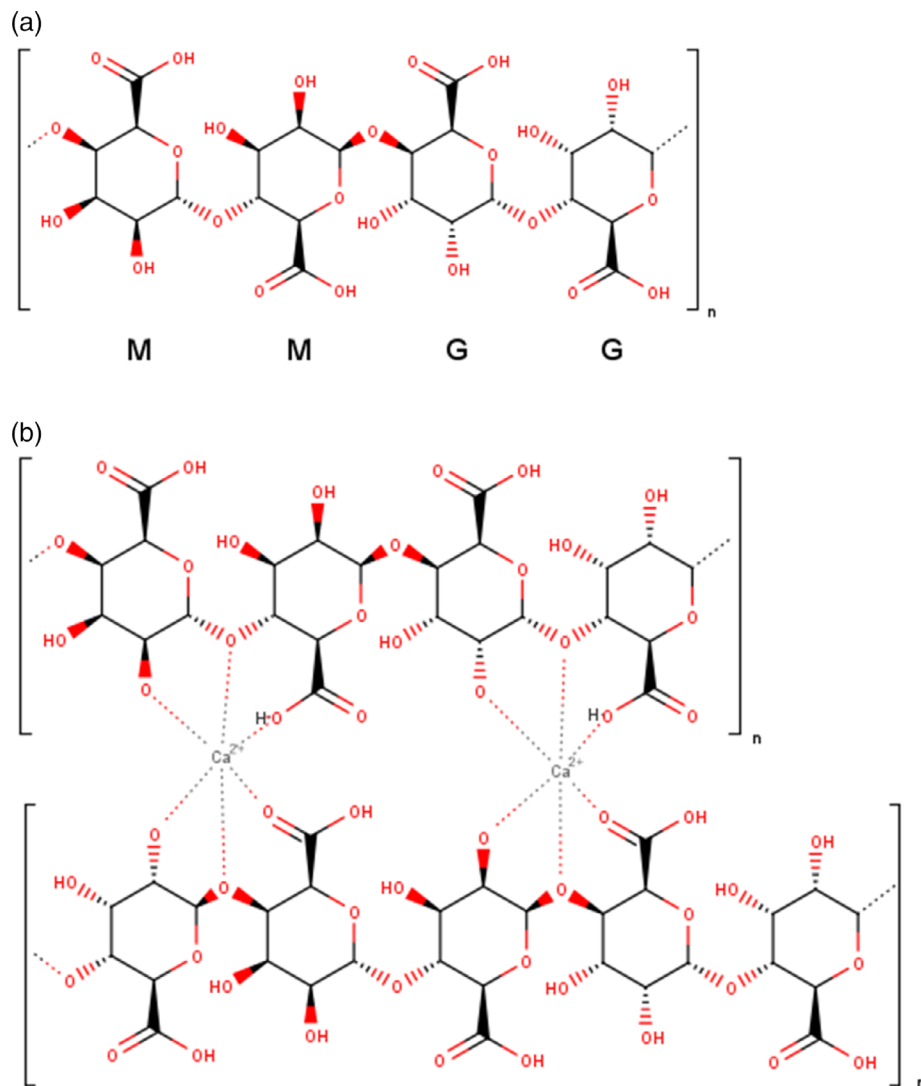


FIGURE 1 Chemical structure of alginate in (a) monomer and (b) cross-linked form [Color figure can be viewed at wileyonlinelibrary.com]

is applied to the alginate hydrogel, the free Ca^{2+} cation forms a coordination bond with the exposed lone pairs of the $\text{C}=\text{O}$, $\text{C}-\text{O}-\text{C}$, $\text{C}-\text{O}-\text{H}$ groups of alginate acid, thus linking various segments alginate acid chains together, resulting in an “egg box” structure,¹¹ Figure 1b. A variety of different factors can affect the physical characteristics of alginate polymers. Such factors include the molecular weight, ratio of M/G, variations in M/G patterns and, block lengths.¹² Not only do these factors correlate to the physical properties of the alginate polymer, they also directly affect the potential applicability of the polymer. This occurs as a result of various parameters being affected such as pore size, pore distribution, matrix composition and swelling capacity, which can affect the polymers applicability as a drug delivery vehicle or as a biomedical scaffold.¹³ While these factors determine the applicability of the polymer for use post-process, the innate properties of alginate also play a significant role.

Alginate wafers are highly desirable due to a variety of innate properties including their hydration capacity, hemostatic properties, mechanical modifiability, and biocompatibility.¹⁴ Hydration capacity stems from the plethora of OH^- groups that allow the molecule to dissociate in water, however when these electronegative regions are coordinated to Ca^{2+} , the dissociability is drastically reduced leading to an insoluble polymer matrix. The hemostatic properties of cross-linked alginates in wound healing occur as a result of the wound exudate being absorbed into the alginate matrix which results in the cross-link dissociation back into alginate acid and Ca^{2+} . Due to the diffusion gradient between the wound and the hydrated alginate, Ca^{2+} cations are absorbed into the wound which facilitates the clotting process,¹⁵ while the Na^+ from the exudate replaces some of the Ca^{2+} , resulting in the formation of sodium alginate. This cross-link process also plays into the aspect of mechanical modification, as cross-link density correlates with rigidity of the

alginate matrix, which in turn can affect the final application of the fabricated alginate polymer. The final factor that determines the application of the polymer is the morphology of the matrix, which in the context of wound healing, should have a high ratio of surface area to volume, which will allow for increased drug loading and controlled release, as well as increased rates of exudate absorbance.

For the purposes of this experiment, the intention is to fabricate the alginate polymer in the form of a wafer, which is ideal for its application toward cutaneous wound healing.¹⁶ This will ultimately help to establish the optimal fabrication method needed for the development of an effective multipurpose alginate platform that can be adapted to any wound healing scenarios.

The specific test parameters within this experiment include the effects of cross-link time, as well as the order of application with respect to freeze-drying and cross linking. The primary focus is to deduce whether or not the variations in the order of application with respect to freeze-drying and cross-linking will affect the mechanical and morphological viability of alginate as a wound healing medium. This is generally not taken into account during the standard fabrication of calcium alginate, which exposes unprocessed bulk sodium alginate to calcium cations.^{17–19} The implication of this study is to help determine the necessary alterations required to produce an alginate wafer that is mechanistically and morphologically appropriate for wound healing. The factors that need to be taken into account include the fact that the alginate wafer needs to be durable enough to withstand repetitive motions presented by various joint movements and also needs to have the correct morphology so as to optimize its applications.

2 | MATERIALS AND METHODS

2.1 | Materials

Sodium alginate powder (216.12/mol) (CAS:9005-38-3), 99.95% D₂O and calcium chloride pellets (mw 110.98 g/mol) were sourced from Sigma-Aldrich, UK. Falcon 35 mm Petri dishes 353,001 sourced from Corning, 3 ml plastic syringe sourced from Fisher Scientific, Microlance 3 needles were sourced from BD.

2.2 | Methods

2.2.1 | Wafer formulation

Both B1 and B2 alginate batches were formed through the solvation of 3 g sodium alginate in 40 ml of deionized

water, stirring for 45 min at 80°C. The resultant polymer solution of 7.5% (w/v) was dispensed into 35 mm Petri dishes in 3 ml portions, which created 1 sample batch and were left to acclimatize for 24 h under standard conditions. A 0.1 mol calcium chloride cross-linking solution was formed via the solvation of 3.685 g calcium chloride pellets in 250 ml deionized water, stirred for 30 min at room temperature.

The B1 alginate wafer batches were formed by first submerging a batch 3 ml polymer solution into the calcium chloride cross-link solution. Each polymer sample was removed at 3-min intervals resulting in 10 different samples of differing exposure times (3, 6, 9, 12, 15, 18, 21, 24, 27, and 30 min). After the cross-linking process, the samples were washed with distilled water to remove excess calcium cations before they were then frozen in a –21°C LEC Medical Freezer LSF39UK for 2 days prior to the freeze-drying process. All samples from the batch were subjected to 0.3 bars of pressure at –52°C in a Christ Alpha 1–2 LD plus freeze dryer for a period of 72 h which ensured the complete desiccation of each polymer matrix.

The B2 alginate wafer batches were formed by first freezing the samples at –21°C for 2 days, before undergoing the freeze-drying process at 0.3 bars and –52°C for a period of 72 h. The desiccated polymers were left to equilibrate at room temperature before their subsequent submersion in the 0.1 mol calcium chloride solution for the intervals of 3, 6, 9, 12, 15, 18, 21, 24, 27, and 30 min. After cross-linking, the polymers were washed with deionized water to remove any excess calcium cations before undergoing freeze drying for 24 h to remove the excess liquid. This in turn inhibits uncontrolled polymer shrinkage, which occurs due to the evaporation of water within the polymer matrix.²⁰

2.2.2 | Microscopic evaluation

Images were taken on a Nikon D750 using a 20 mm f/2.8 prime lens at *f*/8 1/160 s iso100 in conjunction with a 12 mm + 20 mm extension tube. Figure 2 images were taken after 72 h of dehydration in the open air under standard pressure and room temperature. Figure 3 images were taken after the samples were left to hydrate for 3 h in 5 ml deionized water.

In Figure 4, polymer wafers were fully desiccated for 2 weeks prior to scanning electron microscopy analysis. Ten samples of increasing cross-link time from both B1 and B2 batches were analyzed via a TM3030 Hitachi tabletop microscope, with all 20 images taken on the energy-dispersive X-ray imaging mode under high vacuum, with the secondary electron detector set at standard mode.

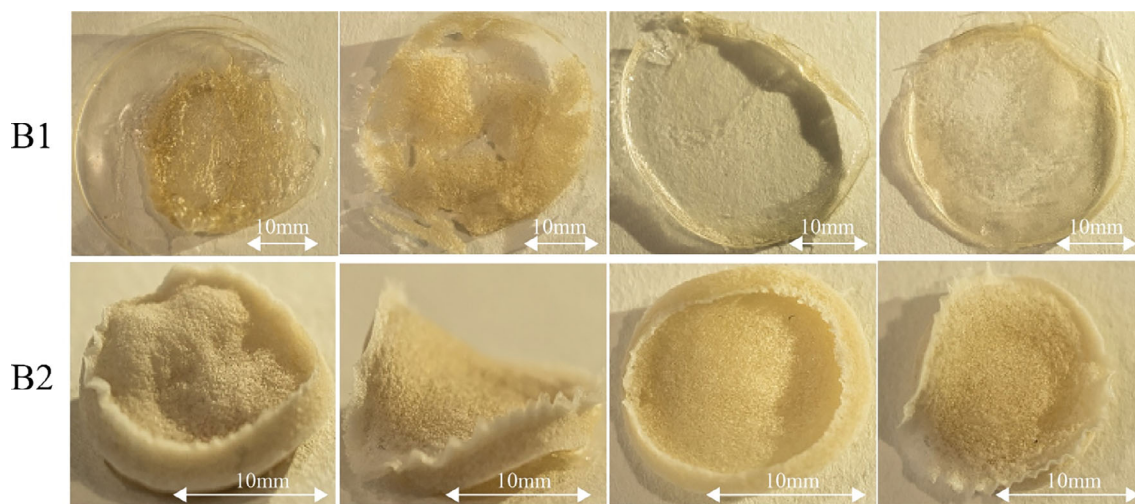


FIGURE 2 Images of 2-week-old air-dried wafers prepared through B1 (freeze drying post crosslinking) and B2 (freeze drying pre cross-linking) [Color figure can be viewed at wileyonlinelibrary.com]

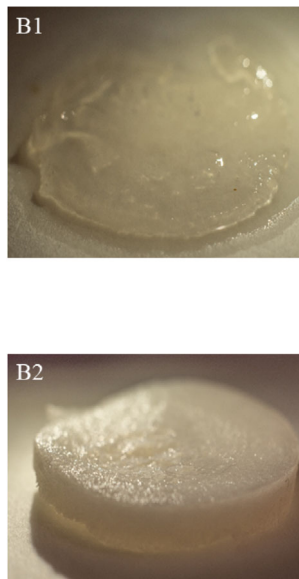
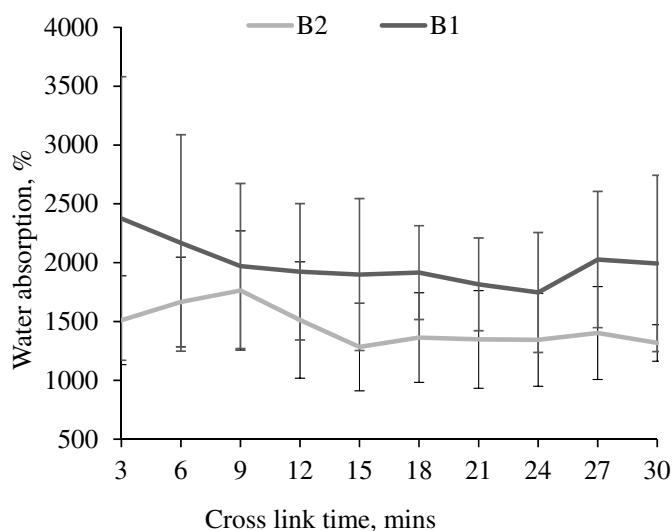


FIGURE 3 Swelling capacity for samples fabricated through the B1 methodology and B2 methodology. a) Water absorption change dependent on cross-link time, b) representative images of 1) B1 and 2) B2 after 1 hour submersion in distilled water [Color figure can be viewed at wileyonlinelibrary.com]

2.2.3 | ^1H NMR measurement

Sodium alginate obtained from sigma-Aldrich was dissolved in D_2O , which was then analyzed in a Bruker AVIII-HD-500 NMR Spectrometer to determine the M/G ratio. The sample was analyzed at 353 K under standard pressure, whereby 128 scans were conducted with a relaxation delay of 2 s coupled with a scanning frequency of 500 MHz.

2.2.4 | Hygroscopicity measurement

The B1 and B2 batches were weighed on a Sartorius CPA224S analytical balance, then left in open air at room

temperature, and standard pressure for 72 h in which they were reweighed to measure the atmospheric water absorption of the polymer. Triplicate tests were conducted on all 10 samples of increasing cross-link time from B1 and B2 batches, resulting in the measurement of 60 samples.

2.2.5 | Hydration measurement

Triplicate tests were conducted on 10 samples of increasing cross-link time for both B1 and B2 batches, where the samples were first weighed to determine their dry weight, before being submerged in distilled water for 1 h at room temperature. Excess water was extracted with a needle

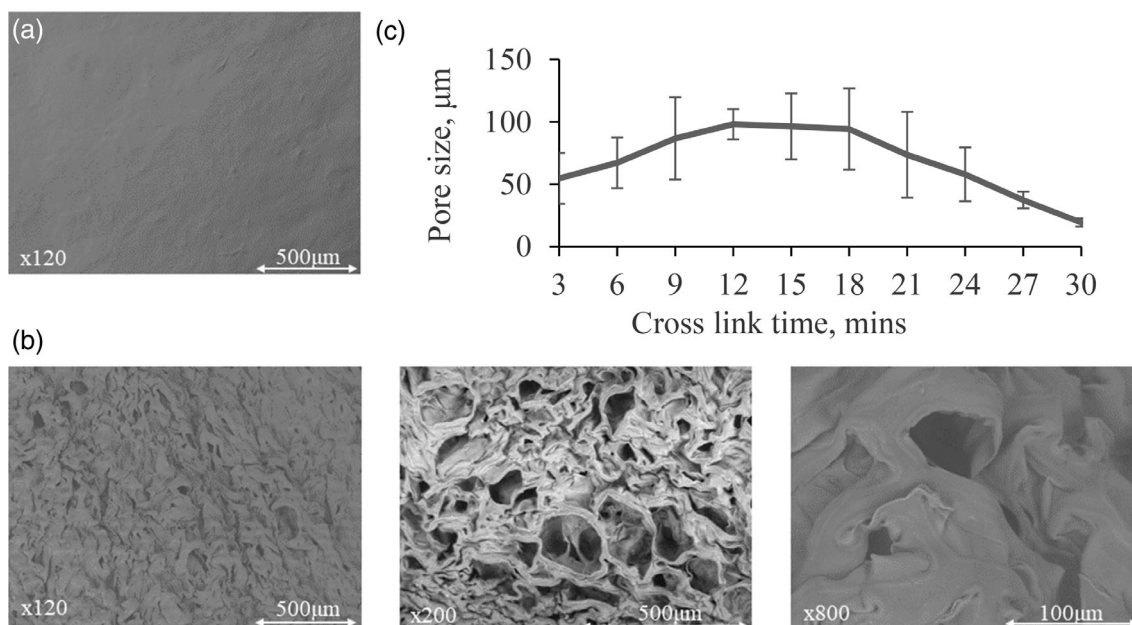


FIGURE 4 Scanning electron micrographs of a) B1 and (b) B2 prepared samples, detailing the overall topography and porosity of both samples, with B1 samples showing no discernible topographical elements, while B2 samples, shown at varying degrees of magnification, display a vast array of pores and fibrous undulations. (c) Average pore diameter data from the B2 samples at varied cross-link times

and syringe prior to the weighing of the hydrated samples.

2.2.6 | Rheological analysis

Triplicates of the 10 samples of increasing cross-link time from both B1 and B2 batches were first hydrated for 2 h at room temperature and standard pressure, before being patted dry to remove excess moisture, thus allowing sufficient grip between the sample and the plates. The sample then undergoes an oscillatory amplitude sweep on the HAAKE MARS rheometer by Thermofisher, between the 0.1 and 60 Pa shear stress under standard temperature and atmospheric pressure. The gap height for batch B2 and B1 samples was set at 0.2 mm with a frequency of 1 Hz to determine the storage modulus G' and loss modulus G'' , whereby 40 time points were taken to deduce any noticeable trend in data.

2.2.7 | Fourier transform infrared spectroscopy

Twenty samples were analyzed using the ATR technique via a Nicolet iS5 FTIR by Thermofisher. Prior to FTIR analysis, the samples were air dried at room temperature, under standard atmosphere for 2 weeks, before being ground down using a pestle and mortar. The fully

dehydrated samples were clamped down until 16 scans were taken per sample following background correction.

2.2.8 | Differential scanning calorimetry and Thermogravimetric analysis

Samples of 3-min, 15-min, and 30-min cross-link time were obtained from method B1 and B2 and were dehydrated for 2 weeks in open air at room temperature under standard atmosphere. The samples were ground down and weighed between 5 and 10 mg before they were then analyzed via both methods. DSC protocol followed the use of a $5^{\circ}\text{C}/\text{min}$ ramp to 250°C from 20°C under standard air 40 ml/min, before undergoing isothermal for 30 min. The temperature was then ramped down via $5^{\circ}\text{C}/\text{min}$ from 250°C to 20°C .

TGA protocol followed the use of $5^{\circ}\text{C}/\text{min}$ ramp to 300°C from 20°C , before an isothermal period of 5 min was held.

2.2.9 | Evaporative water loss

Three sets of B1 and B2 samples contained within 35 mm Petri dishes were immersed in 8 ml of deionized water for 24 h at room temperature and standard atmosphere, with the lid cover placed on top. After immersion, excess water was blotted away leaving only the samples in their

hydrated state. These samples were weighed and then air dried at room temperature with the lid cover off for 24 h before the samples were then reweighed.

3 | RESULTS AND DISCUSSION

The study was conducted to identify the effects of cross-link time, as well as the order of application with respect to freeze drying and cross-linking on the mechanical and morphological properties of the alginate wafers. The aim was to identify the specific effects of these parameters on the physical properties of the wafers, which would then allow for these wafers to be optimally fabricated relative to their applications, that is, wound healing.

Alginate wafers were successfully produced for both B1 and B2 methodologies, whereby the difference in the B1 and B2 fabrication procedures produced vastly different macrostructures, as shown in Figure 5, B1 wafers are of a 3 dimensionally flat morphology and are either translucent or transparent, relative to the amount of unbound alginate that is directly below the cross-linked layer (Figure 2). Method B2 on the other hand produces a matrix with more thickness and is opaque relative to the B1 morphologies. Two main morphologies exist for B1, as shown in Figure 2, either non-uniform patches of cross-linked alginate or a fully transparent thin top layer of cross-linked alginate with

bulk non-cross-linked alginate aggregating around the outside. In both cases, the thickness of the B1 wafers was thinner than their batch 2 counterparts. The B2 wafers possessed a more substantial three-dimensional matrix structure which is predominantly a result of the matrix being locked in place via cross-linking before it is affected by the suction forces generated by the freeze dryer. In the specific case of B1 samples, its morphology occurs as a result of the suction forces acting on the uncross-linked alginate which then lost its structural integrity as it began to melt. This is demonstrated by Figure 6 which depicts the transition in its morphology throughout the freeze-drying process. In some cases, the structure develops a slight curvature which occurs as a result of the polymer strands shrinking relative to the removal of moisture. This curvature can prevent the matrix from expanding uniformly during the hydration process, which may prevent it from correctly conforming to the wound. This in itself reduces the immediate contact area between the matrix and the host's exudate, thereby limiting the rate of exudate absorption and therapeutic drug release.

3.1 | Microscopic analysis

The wafers were imaged using scanning electron microscopy (SEM) to image their microstructure and estimate

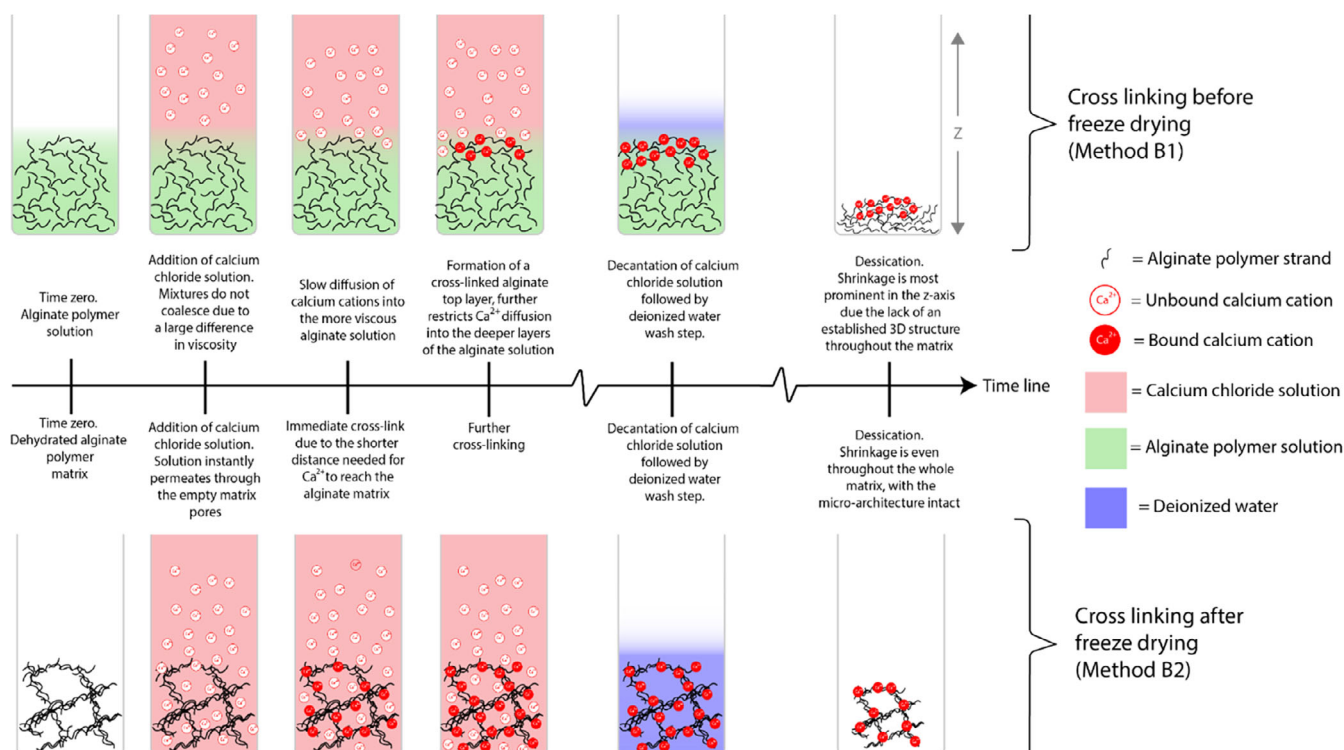


FIGURE 5 Illustration depicting the structural differences of the final products fabricated as a result of method B1 and B2 [Color figure can be viewed at wileyonlinelibrary.com]

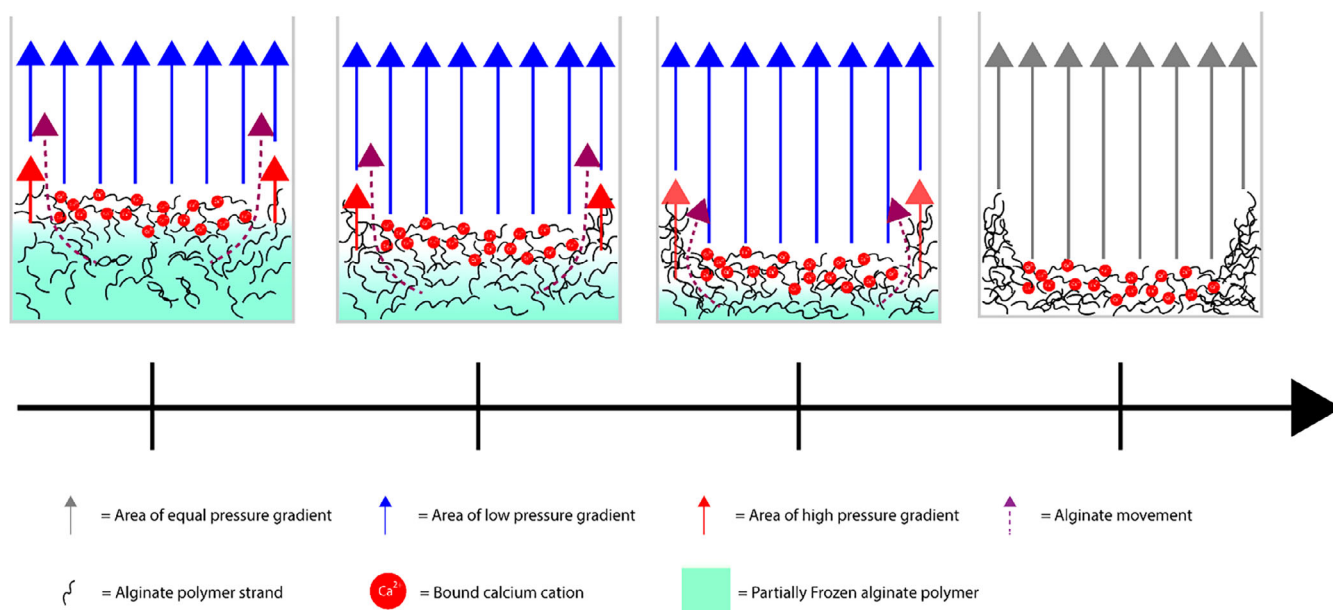


FIGURE 6 Detailed illustration depicting the effects of freeze-drying process on a pre-crosslinked alginate [Color figure can be viewed at wileyonlinelibrary.com]

their pore sizes. The B1 wafers did not produce any visible pores at any of the any cross-link durations with a representative image being shown in Figure 4a. Here, the surface is very smooth with very few distinct features, none of which could be identified as a pore. Based on the fact that method B1 cross-links the alginate before freeze drying, it is therefore expected that the top layer is heavily cross-linked to the point where it inhibits the diffusion of calcium cations beyond the cross-linked layer. The B2 wafers possessed a matrix with a uniform yet disordered structure, whereby it is quite clear that the alginate strands that are bound together have contracted as a result of dehydration, resulting in a morphology with high degrees of curvature as observed in Figure 4b. In terms of pore distribution, all the pores were relatively well distributed throughout the matrix without specific areas having larger concentrations of pores relative to one another. Figure 4c demonstrates that the average pore size increased at increasing cross-linking times up to 12 min, where they then slowly shrink until the 18 min mark, after which a rapid shrinkage occurred. Based on the error bars, it can be observed that the pore size is generally quite inconsistent prior to 27 min, with exception for 12 min which has a smaller fluctuation in size relative to the other values. Beyond 24 min the fluctuations in pore size drastically decreases. The range of pore sizes is between 19.3 and 98.1 μm , which is larger than that of those found in literature,^{21–25} however this is due to the fact that most literature utilizes a lower alginate w/v ratio of below 3%, which would imply higher concentrations of water within the alginate matrix and

would therefore have more points of ice crystal nucleation. This in turn would result in a higher abundance of small pores, whereas a higher alginate w/v ratio would result in a lower relative abundance of larger pores.

It should be noted that the main factors affecting the final pore size for B2 wafers is attributed to the formation of ice crystals, dehydration, and cross-link time. The nucleation of ice crystals provide the initial expansive forced need in the formation of the pores, which are then generated through the sublimation of said ice crystals. The final size of the ice crystals prior to sublimation determine the maximum size of the pores, whereby the removal of the ice crystals then allows for the facilitation of dehydration induced contractual forces to uniformly shrink the matrix.

For the aspect of wound healing, the release of calcium cations from calcium alginate help to facilitate hemostasis, while the polymer matrix helps with the aggregation of erythrocytes and platelets by providing a physical scaffold for cellular adhesion.²⁶ In this context, B2 30-min cross-link samples will provide the smallest pore size, which in turn will provide the largest surface area-to-volume ratio, thereby maximizing the quantity of cellular aggregation in a uniform manner. It should also be noted that B2 30-min cross-link samples will also have the highest loading of calcium cations, which in turn will extend the therapeutic dosage window for hemostasis to occur. The main clinical implications of the B2 30-min cross-link samples lie in the fact that the platelet plugs will form uniformly within the smaller pores, which overtime expand to form one large consistent plug. This

occurs as a result of the calcium cations being released from the alginate as it contacts the host's bodily fluids, resulting in its structural breakdown as it contacts the host's bodily fluids, causing Ca^{2+} and Na^+ exchange to occur between the matrix and bodily fluids, respectively.²⁷ Overtime, this causes the Ca^{2+} within the matrix to be gradually replaced by Na^+ thereby allowing further platelet aggregation to occur around the plug in place of the broken down alginate.

3.2 | Hygroscopic measurements

Hygroscopic weight measurements help to identify the magnitude of atmospheric moisture absorption by the wafers. This plays a role in the degradation of the product as the introduction of water into a desiccated structure increases its entropy leading to increased rates of degradation. The hygroscopicity data, Figure 7, indicated that the process of cross-linking after freeze drying (B2) reduced the hygroscopic moisture gain from the local environment compared to the B1 method.

The difference in average weight gain from atmospheric water absorption between B1 and B2 samples were very small, whereby the maximal difference in average hygroscopic gain between B1 and B2 samples occurs at the 3-min cross-link mark with an average difference of 0.073589 g which equates to a percentage difference of 28.6%. For both B2 and B1 batches, there is a weak negative correlation in regards to the decrease in hygroscopic gain relative to cross-link time. Based on the trendlines, it is clear that cross-link time impacts atmospheric weight gain more heavily for B1 samples than B2 samples, as shown by $-0.0023 \times$ and $-0.0004 \times$ trendline values with respect to B1 and B2. Due to the fact the hygroscopic differences between both methods are quite minimal, coupled with the general minute gain in moisture content, the implications are that the methods themselves

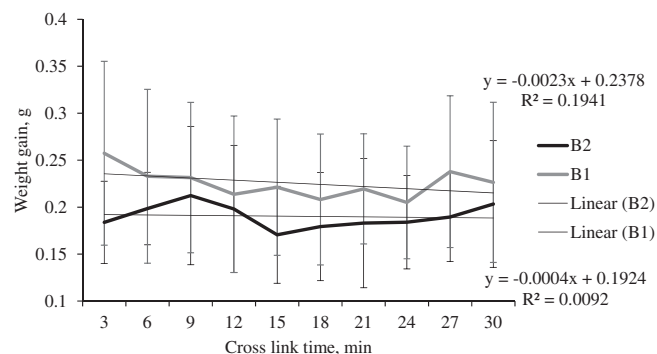


FIGURE 7 Changes in weight for samples fabricated through the B1 and B2 methodology

have minimal effect in regards to hygroscopic analysis. Despite the negligible differences in hygroscopicity, it is quite clear that the application of freeze drying prior to cross-linking reduces the fluctuation in hygroscopic gain, especially in regards to the shorter cross-linking time periods which may be due to the increased permeability of method B2. The implications of the B2 method may be that it narrows down the fluctuations in value by facilitating a very steady rate of cross-linking unlike that of method B1 which only cross-links the top layer, thereby allowing the hydrogel below to partake in more hygroscopic gain. Assuming that the fact that method B2 produces a larger volume of Ca^{2+} facilitated coordination bonds relative to method B1, it can be implied that the B1 samples would therefore have more unoccupied OH and =O bonds. This in turn would allow more hydrogen bonding to occur between the unoccupied bonds and atmospheric water, resulting in increased mass gain, which would explain why B1 has a higher hygroscopic gain relative to B2. Relative comparison against literature shows that the hygroscopic gain from both B1 and B2 methodologies at room temperature fall in line with the minute gain in mass from other calcium alginate tests.²⁸

3.3 | Hydration measurement

Swelling capacity is the measurement of maximal water absorption within a material. Based on Figure 3a, method B2 gives a more consistent set of data values relative to method B1, which possesses large fluctuations in swelling capacity. The fluctuations in method B1, especially between 3 and 6 min cross-link time, occur as a result of unbound alginate being hydrated and detaching from the main freeze-dried bulk matrix. The unbound alginate when hydrated swells and diffuses into the excess body of water, this makes it exceedingly difficult to separate during the removal of excess water before swelling capacity weight measurements. Due to this reason the swelling capacity of method B1 is especially varied for the lower cross-link durations. The difference in both hygroscopicity and water swelling indicate that the initial cross-link process in Batch 2 occurs at a higher rate and in a more uniform fashion, leading to the occurrence of more ionic bonds within a set time frame, subsequently leading to less OH^- available for hydrogen bonding with water. The physical appearance of the samples were in agreement with these findings, whereby, the B2 wafers matrices return to a uniformly flat morphology once they are rehydrated, (Figure 3B2) whereas the B1 wafers (Figure 3B1), formed a semi-gelatinous solution.

Literature has shown that calcium alginate's water absorption capacity is around 1500–1700%, which is similar

to the results from method B2, but is substantially lower than that of method B1.²⁹ Overall, both fabrication methods indicate that there is a weak negative correlation in regard to the swelling capacity as a function of cross-linking time. Comparatively speaking B2 samples had a lower capacity for hygroscopicity and water swelling which agrees with the assumption of Ca^{2+} ionic bonding limiting the numbers of available OH^- lone pairs for hydrogen bonding with free water molecules. Based on the fact that B2 possessed lower average hydroscopic gain, this suggests that the uniform distribution of cross-linking reduces the total water absorption capacity as a result of more OH and =O groups within the alginate being occupied by the Ca^{2+} ionic bond, which in turn, drastically reduces the amount of hydrogen bonding with unbound water, thus decreasing the dissociability of the polymer matrix.³⁰ The main limitation of this study lies in the fact that the B2 matrices when

dehydrated in open air, after cross-linking, take upon a slightly different morphology with respect to the cross-link time. This is to be expected given the fact that increased cross-link results in more anchor points for which dehydration induced contraction can occur, resulting in more extreme curvatures when the matrix is fully desiccated. This limitation could potentially affect the rehydration rate of the alginate matrix; however, this may be mitigated by applying a flat weight on top of the matrix during the dehydration process, thus resulting in a flatter morphology for all the B2 matrices.

3.4 | Rheological analysis

The storage modulus (G') and loss modulus (G'') profiles presented by methods B1 and B2 (Figure 8), demonstrate

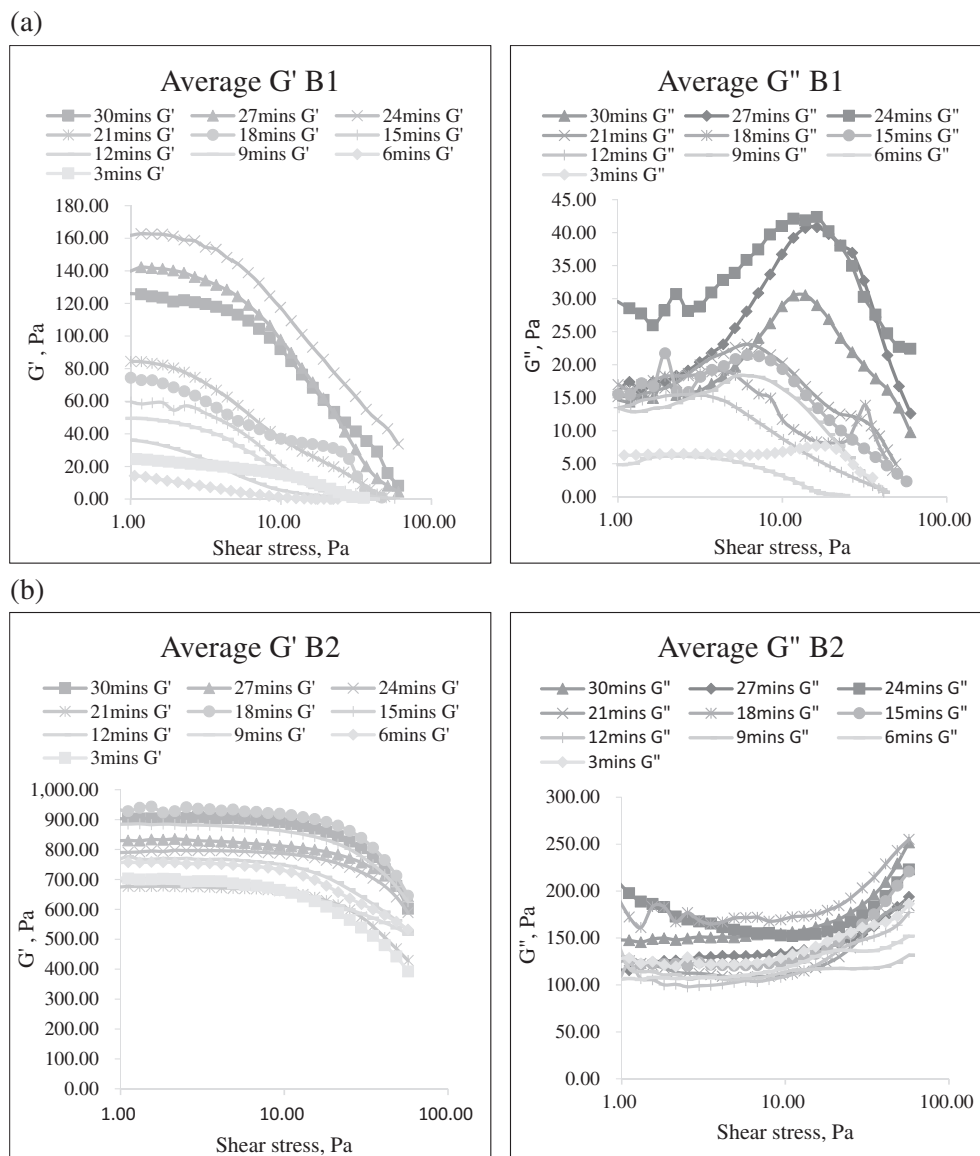


FIGURE 8 Average change in G' and G'' for (a) B1 and (b) B2 prepared samples

that there is a clear distinction in terms of relative separation and the nature of its relationship to the increase in shear stress. The B1 wafers G' undergoes a decay profile similar to that of an exponential profile, whereas the B2 wafers possess G' readings similar to that of logarithmic decay. In general, the G' and G'' of the B1 wafers are generally lower relative to that of the B2 wafers, whereby a notable difference is observed in the separation between the Pa values of G' and G'' . In general, the greater the separation between G' and G'' , the more solid the object is in terms of its microstructural rigidity relative to the application of external mechanical forces. In this regard it is quite clear that despite the large fluctuations of the G' values in the B2 wafers relative to the B1 wafers, the value differences in Pa between G' versus G'' for B2 wafers is still dramatically larger than that of the B1 wafers. Whereby the smallest difference between G' and G'' for the B2 wafers is 205.56 Pa which is still larger than that of maximal Pa difference in the B1 wafers which is 136.49 Pa.

The relative comparison of both G' and G'' values can be used to identify their change in phase angle as a function of time, as shown in Figure S1. The contrast in phase angle measurements between the B1 wafers and the B2 wafers is very distinct, whereby B2 wafer phase angle measurements are generally more consistent, following a slow, but strong increase in phase angle as a function of shear stress. The phase angle of the B2 wafers do not exceed the yield point of 45° , thereby implying that all the B2 wafers, even with minimal cross-link time are of a strong solid state. For B1 wafers, the phase angle measurements on the other hand are erratic, with many samples exceeding the yield point below 40 Pa shear stress, implying that their transition into a more viscous dominant state is generally more prevalent. The B2 wafers phase angle measurements did not seem to be affected by cross-link time, as no discernible trend in regard to the changes in phase angle as a function of shear stress were observed. Analysis of B1 wafers implied a weak negative correlation whereby the increase in cross-link time results in a smaller phase angle as a function of increasing shear stress. It should also be noted that the B1 wafers at a reduced cross-link time also fail to go beyond a certain shear stress value as some of the samples reach mechanical failure earlier than others. This implied that the samples with a lower cross-link time have a smaller capacity for the storage of mechanical energy and would therefore collapse earlier than their counterparts with a larger cross-link time period. The differences in rheological properties between the B1 and B2 wafers were supported by the complex modulus readings as shown in Figure S2, which demonstrate the rigidity of the material below its yield point. In this regard it is very clear that the B1 wafers are closer to the yield stress and would

therefore illicit traits more similar to that of a liquid, while B2 wafers are firmly within the bounds of being in a solid like state. This is further reinforced by the trends in angular frequency which describes the rate of rotation in radians as a measure of time, Figure S3. The maximal changes in angular frequency for B2 is approximately 0.004 rad s^{-1} , which is notably smaller than that of the B1 wafers, which possessed a maximal change of approximately 0.017 rad s^{-1} . Comparatively speaking, the B2 wafers rate of rotation is much less than the B1 wafers, which further implies the structural superiority of the B2 wafers.

Based on the observed results it can be implied the distribution of Ca^{2+} cross-links varies greatly between both B1 and B2 methodology, as the B2 samples are able to resist a greater level of shear stress, which in turn would suggest a greater level of uniform mechanical strength. Comparison with literature further reinforces the fact that higher levels of Ca^{2+} presence within the matrix correlates with increased rheological strength, which therefore leads to increased mechanical resistance as a function of increasing mechanical stress.³¹

3.5 | FTIR analysis

Analysis of FTIR data, Figure 9, shows a general shift of major peaks relating to the vibrational activity of OH groups, which is expected as the exchange of sodium cations into calcium cations results in the structural formation following that of the egg-box model, which is composed of chelating and coordination structure.¹¹ As a result of the replacement of Na^+ with Ca^{2+} , the exertion of electromagnetic attraction becomes stronger, which when applied against the hydroxyl groups of alginate will result in the increase in bond length, which in turn results in the shifting of its peaks to a lower wavelength. Analysis of both B1 and B2 data shows that the vast majority of bands were close to identical in terms of their positioning, however the biggest observable differences lie in their transmittance percentage relative to one another.

Based on Table 1, the broadest and roundest band occur at $3000\text{--}3650 \text{ cm}^{-1}$ signifying the stretching vibration of O—H bonds, next to this band is the $2850\text{--}2980 \text{ cm}^{-1}$ band represents the C—H from the pyranose ring. The next set of bands occur between $1500\text{--}1700 \text{ cm}^{-1}$ and $1350\text{--}1500 \text{ cm}^{-1}$ which signify the shifted asymmetric and symmetric stretching vibrations from carboxyl C=O respectively, both of which have occur as a result of its formation as a carboxylate salt ion complex.³² A small peak occurs at $1250\text{--}1350 \text{ cm}^{-1}$ which represents CCH + OCH, while $1050\text{--}1100 \text{ cm}^{-1}$ represents the OCO group within the pyranose ring.

The final bands occurs at $950\text{--}1150 \text{ cm}^{-1}$ which represents the vibrational stretch of the C-O groups within

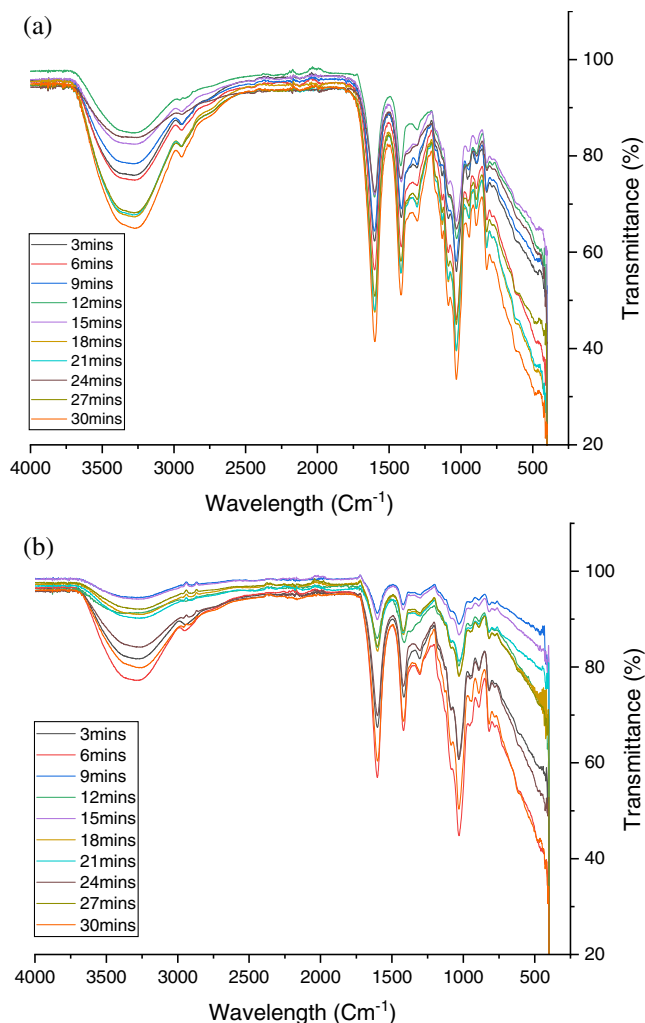


FIGURE 9 FTIR transmittance as a function of cross-link time and preparation method for (a) B1 and (b) B2 prepared samples [Color figure can be viewed at wileyonlinelibrary.com]

TABLE 1 Assignment of vibrational modes for calcium alginate

Vibration	Position (cm ⁻¹)
O—H	3000–3650
C—H—Anomer	2850–2980
COO—Asymmetric	1500–1700
COO—Symmetric	1350–1500
CCH + OCH	1250–1350
OCO—Ring	1050–1100
CO—Stretching	950–1150
CO—Stretching uronic acid	920–980

the pyranose rings and the 920–980 cm⁻¹ CO uronic acid stretch. The observed band positions were consistent with other calcium alginate FTIR data from literature.^{32–34}

Overall, the majority of peak positions between all the samples were identical, with the exception of a few cases, whereby slight variations in the visibility of certain peaks seem to differ between samples. This includes B2 6 min, OCO peak is not as prominent due to it being overshadowed by the CO stretching vibration. This does not occur for sample B1 6 min but appears for samples B1 12 and 24 min. Another slight difference occurs at the CCH + OCH vibration whereby B2 12 min and B1 24 min does not display a visible peak, unlike all the other samples where it is easy to identify. The biggest difference between B1 and B2 samples with respect to peak positions occurs at the CO uronic acid stretch, which has the greatest variation in terms of slight shifts that occur. B2 samples with respect to the CO uronic acid stretch were all aligned to 918 cm⁻¹, however B1 samples shows significant variations, with most aligning at 940 cm⁻¹. The outliers of B1 include 6 and 3 min which is shifted to 960 cm⁻¹, 12 min which is shifted to 950 cm⁻¹, 15 min which has a broader than average peak of 940–960 cm⁻¹ and 24 min which does not show the peak at all. Going with the assumption that B2 produces equal distributions of Ca²⁺ crosslinkers, it would therefore explain why all the B2 peaks would be equally shifted and therefore all aligned. On the contrary, B1 samples with their non-homogenous distribution of Ca²⁺ crosslinkers, would therefore result in disproportionate formations of carboxylate salt ion complexes throughout the matrix, which would in turn result in no shifting if the b1 sample piece have very little to no Ca²⁺ present within it.

Comparison between the two data sets presented by Figure 9a,b which are methods B1 and B2 respectively, we can see that the transmittance percentage is significantly lower in B1 which implies that there is a relatively larger population of bonds that have the same vibrational energy with respect to the incident light. In the case of B2 samples, it would imply that there is a comparatively smaller population of bonds, which may be indicative of the number of Ca²⁺ cross-links that have occurred.

This is suggested by the comparison of B1 sample data with the of FTIR literature of sodium alginate,³² both which bear a very similar set of band positions and transmittance percentage relative to one another. Based on this it could be implied that the sodium alginate makes up the majority of the B2 population, which in turn would suggest that the presence of Ca²⁺ cross-linking is lower for that preparation method.

3.6 | DSC and TGA analysis

Comparing the differential scanning calorimetry (DSC) and thermogravimetric analysis (TGA) data from

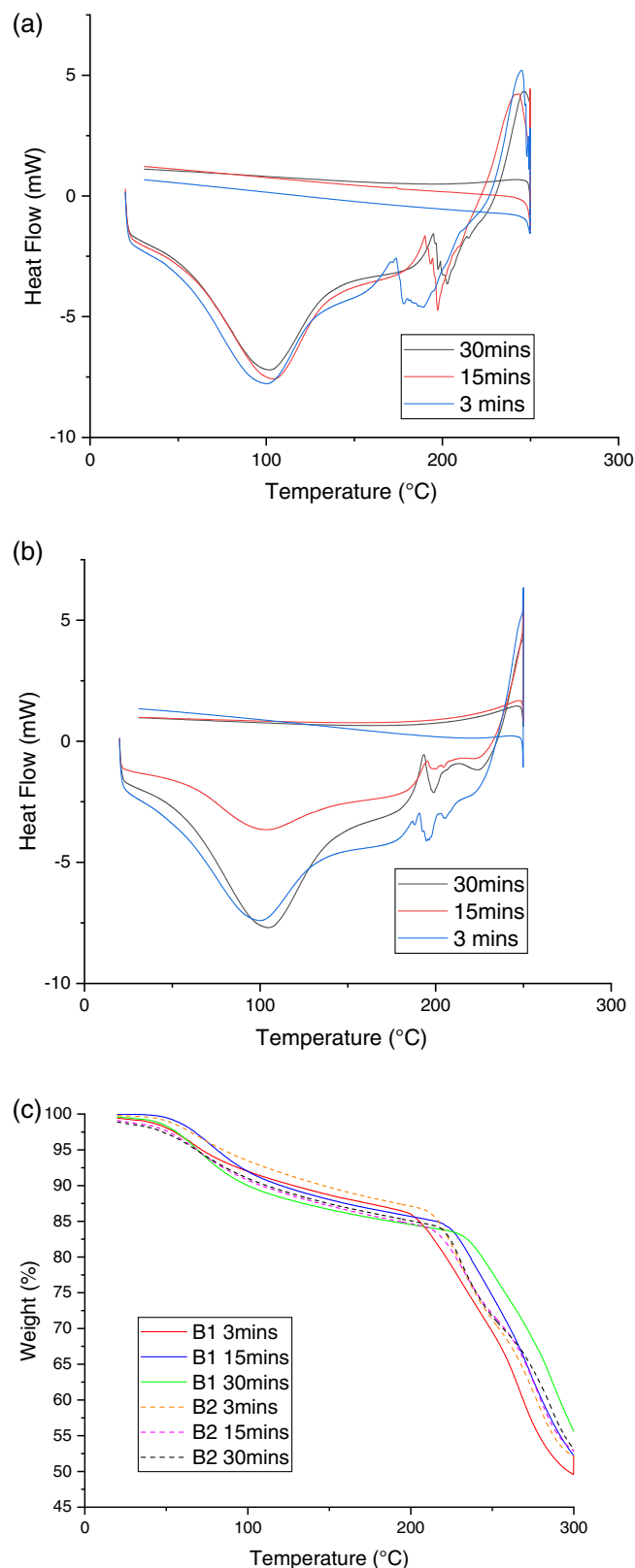


FIGURE 10 Heat flow changes for (a) B1, (b) B2 prepared samples with respect to cross-link time, and (c) comparison of weight loss changes as a function of temperature [Color figure can be viewed at wileyonlinelibrary.com]

Figure 10 of both method B1 and B2, there were some distinct similarities and differences. In terms of the TGA data, both B1 and B2 samples follow a similar downward trend, where there is a relatively steep slope between 50°C and 100°C as the unbound water gets evaporated off of the alginate matrix. Beyond that point, there were slight variations in temperature points with regards to the breakdown of the ionic cross-link which is represented by the first minor dip after 170°C. In regards to the DSC data, the initial peak in heatflow of the aforementioned dip represents the maximal endothermic exchange before the thermolytic cleavage of the carboxylate salt ion complex, which is represented by the drop in heatflow, thus signifying an exothermic reaction. A sharp dip is indicative of highly crystalline structure, which in the case of calcium alginate, would be the “egg box model”.¹¹

For method B1 3-min the dip begins at 175°C, 15-min 192°C, 30-min 197°C, while for method B2 3-min, the dip begins at 191°C, 15-min 197°C and 30-min 193°C. Comparatively speaking, method B2 has a more consistent endothermic peak with respect to temperature, whereas for method B1, there is a larger discrepancy in the consistency of the ionic endothermic peak, with the B1 3-min cross-link sample undergoing its endothermic exchange at a lower temperature. Literature identifies the calcium alginate endothermic dip to occur at 197°C and 194.05°C, with sodium alginate lacking this specific dip.^{35,36} This would therefore imply that both samples, irrespective of cross-link time, were both calcium alginate, possibly suggesting that the occurrence of B1 3-min dip at 175°C is as a result of the reduced quantity of calcium carboxylate complexes formed, which would therefore lead to an earlier exothermic event with respect to the ramp rate. The reason as to why B1 and B2 display similar DSC and TGA results is primarily due to the fact that the B1 process separates the unbound alginate from the cross-linked top layer, as shown in Figure 2, thereby leading to difficulties with respect to producing a small enough sample for measurement that can accurately represents the methodology. This is further compounded by fact that the dehydration process drastically reduces the volume of the unbound alginate, resulting in the majority of the B1 matrix’s volume being predominantly the cross-linked top layer when it is ground down for analysis.

3.7 | M/G analysis

As shown by the ¹H NMR spectra in Figure 11, the sample was heated to 80°C which removes the water peak,

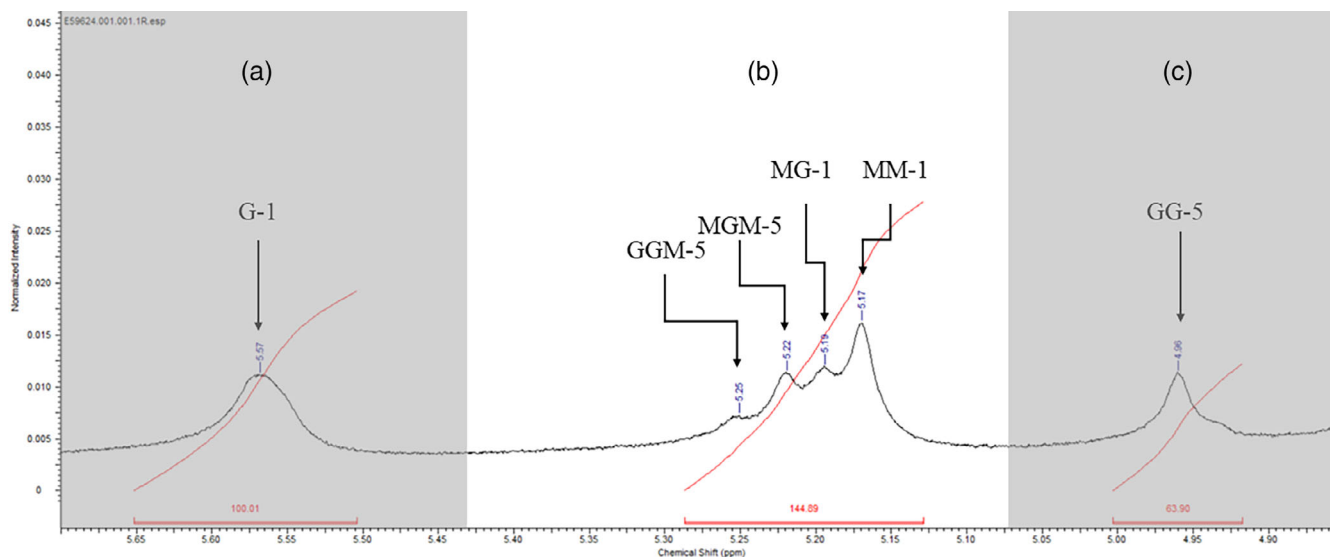


FIGURE 11 Proton NMR spectrum, detailing the various peaks associated with each alginate block. (a) Integrated area of G-1, (b) combined integrated area of GGM-5, MGM-5, MG-1, MM-1, (c) integrated area of GG-5 [Color figure can be viewed at wileyonlinelibrary.com]

which would typically obscure the key signals, but also as a consequence shifted the position of each signal. The primary purpose of this analysis is to deduce the M/G ratio via the relative comparison of the integrated areas G-1 (5.51–6.65 ppm), GG-5 (4.92–5.01 ppm) and the combined areas of GGM-5, MGM-5, MG-1 and MM-1 (5.13–5.29). Integration calculations were performed following the method used by Jensen et al.,³⁷ which gave a M/G value of 1.09.

$$\frac{M}{G} = \frac{B + C - A}{A}$$

This M/G value is relatively low, thereby indicating that this particular batch of sodium alginate would produce polymers that are more brittle, as higher M residue contents produce matrices that are more pliable in nature, while high G residues coupled with long GG blocks result in more rigid matrices.³⁸ When comparing this data to literature that has also characterized Sigma-Aldrich sodium alginate (CAS:9005-38-3), there is a clear indication that there is a batch to batch difference with respect to the M/G ratio, as Belattmania et al., observed a M/G value of 3.42 which were higher than the values observed from this experiment.³⁹ Given the fact that Ca²⁺ primarily binds toward G and MG blocks, the implications with respect to the experimental data would therefore suggest a higher population of G blocks which in itself would imply more cross-linking sites for Ca²⁺. Assuming the fact that the other batches of sodium alginate may have higher M/G ratios, it could then be suggested that the

mechanical strength of the experimental matrix is therefore at the higher end of spectrum, which then gets further pronounced with respect to the increase in cross-link time.

3.8 | Evaporative water loss measurements

Based on the results of Figure 12a, the general trend indicates that there is positive correlation in regards to evaporative water loss relative to cross-link time, whereby B1 has an R^2 value of 0.3944 indicating a weak correlation, while B2 has an R^2 value of 0.5338, which indicates a moderate correlation. Comparison between B1 and B2 results indicate that B2 samples generally undergoes a higher degree of evaporative water loss, with the exception of 3, 9, 12, and 18 min which show similar levels of water loss. It should be noted that B1 samples have larger standard deviations than B2 samples with the exception of 9 and 15 min, as shown in Figure 12b. These large variances may be attributed to the loss in structural integrity as the B1 samples get hydrated and breakdown, leading to changes in total in surface area which affects the rate of water loss. This would be further exacerbated for B1 samples at higher cross-link times due to variations in their final morphology, as shown in Figure 2, which can affect their dissociation in water, thus leading to greater variances in their evaporative water loss values.

On the other hand, B2 samples did not lose structural integrity as a result of the hydration process, with

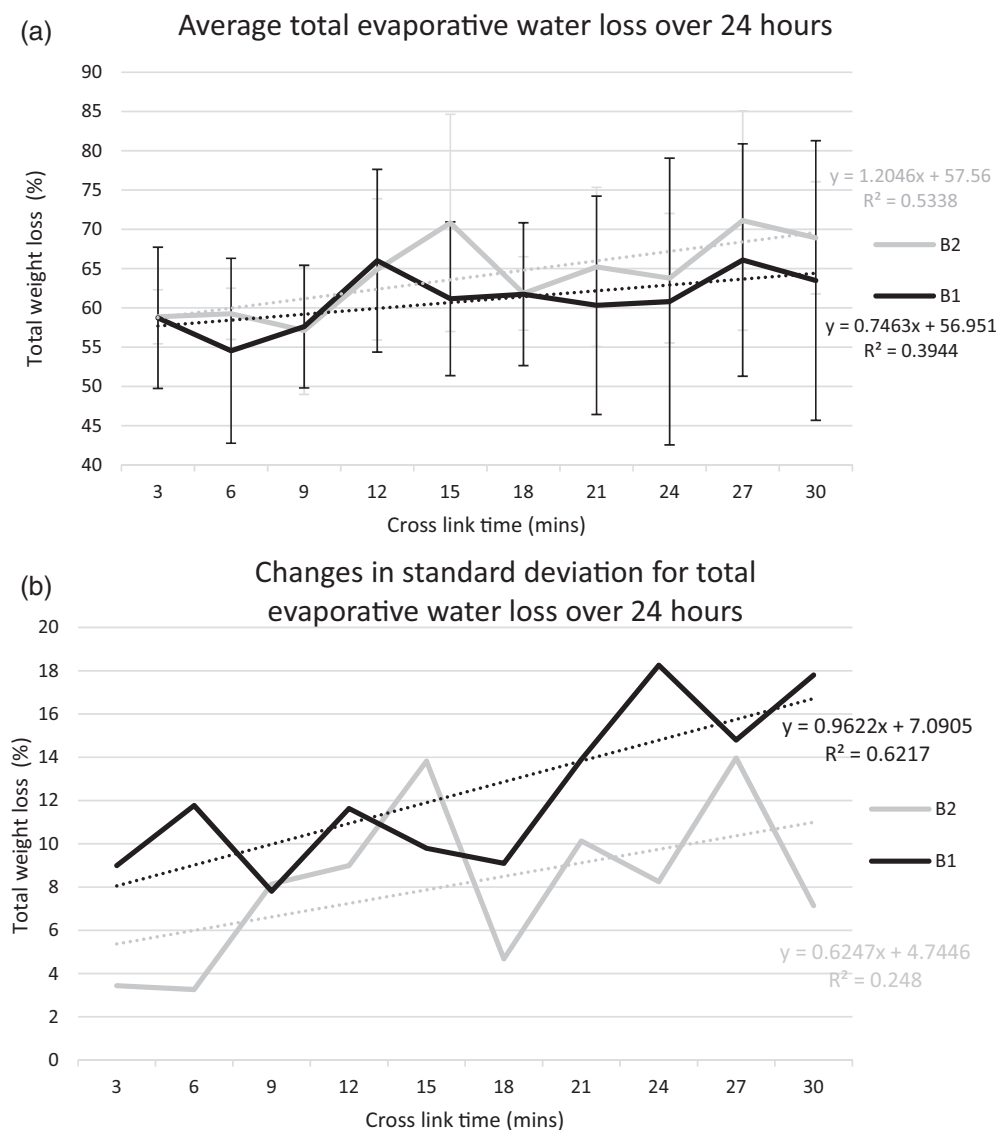


FIGURE 12 (a) Changes in total evaporative water loss over 24 h with respect to increasing cross-link time. (b) Changes in standard deviation for total evaporative water loss over 24 h

respect to the B1 samples, however the standard deviation still increases overall, with 15 min being an anomaly. Based on the results of Figure 12b, there is a moderate positive correlation between increasing cross-link time and increasing standard deviation of evaporative water loss for B1 samples, whereas for B2 samples there is a weak positive correlation. The overall implications suggest that a lower cross-link time may be more appropriate for reducing evaporative water loss, as well as its associated deviations, which would allow for more consistency when applied toward wound healing applications.

4 | CONCLUSION

This study has demonstrated that preparation method for producing alginate or alginate-based wafers with a high

level of structural integrity and optimal rheological properties is vital. In order to fabricate stronger polymer wafers it is necessary to first freeze dry them before the cross-linking step, thus facilitating the uniform distribution of cross-links throughout the polymer system, thereby leading to increased mechanical strength. The key findings from this study imply that the B2 methodology produces polymer wafers with superior mechanical characteristics coupled with a morphology that is more suitable for wound healing applications. The B2 wafers provide increased mechanical strength, porosity and surface area which ensures that the wafer is durable enough to serve as a wound healing platform for increased drug release and exudate absorption without compromising the structural integrity of the matrix. For future studies, it would worth investigating whether or not the distribution of alginate associated cross-links can be affected by the type of multivalent cationic agent that is used, that is,

Zn²⁺ and Ga³⁺. It may also be worth exploring the simultaneous use of two differing multivalent cationic species for alginate cross-linking, as it could potentially give further insight toward the methods in which one could use to manipulate the physicochemical characteristics of the matrix. Assuming that it possible to control the release priorities of differing cationic populations, this could then have significant therapeutic implications as certain cations such as Ca²⁺, Zn²⁺, Fe²⁺, and Mg²⁺ which all have positive therapeutic effects when undergoing controlled release into the body.^{40–42}

AUTHOR CONTRIBUTIONS

Ernest Man: Data curation (lead); formal analysis (lead); methodology (lead); writing – original draft (lead). **Adeolu Oluwasanmi:** Data curation (supporting); formal analysis (supporting); writing – original draft (supporting). **Dimitrios A. Lamprou:** Methodology (supporting); supervision (supporting). **Kirsty Goudie:** Data curation (supporting); formal analysis (supporting). **John Liggat:** Supervision (supporting). **Clare Hoskins:** Conceptualization (lead); supervision (lead); writing – review and editing (lead).

ACKNOWLEDGMENTS

The authors thank the Strathclyde Student Excellence Award for funding this work.

CONFLICT OF INTEREST

The authors would like to state that they have no conflicts of interest.

DATA AVAILABILITY STATEMENT

The data that support the findings of this study are available from the corresponding author upon reasonable request.

ORCID

Clare Hoskins  <https://orcid.org/0000-0002-7200-0566>

REFERENCES

- [1] B. A. Aderibigbe, B. Buyana, *Pharmaceutics* **2018**, *10*, 42.
- [2] N. R. Barros, S. Ahadian, P. Tebon, M. V. C. Rudge, A. M. P. Barbosa, R. Di Herculano., *Mater. Sci. Eng. C* **2020**, *119*, 111589.
- [3] P. Ray, M. Maity, H. Barik, G. S. Sahoo, S. Hasnain, M. N. Hoda, A. K. Nayak, Chapter 3—Alginate-based hydrogels for drug delivery applications. in *Alginates in Drug Delivery*, Academic Press, London **2020**, p. 41.
- [4] K. Chaturvedi, K. Ganguly, U. A. More, K. R. Reddy, T. Duge, B. Naik, T. M. Aminabhavi, M. N. Noolvi, in *Natural Polysaccharides in Drug Delivery and Biomedical Applications*, London, Academic Press **2019**, p. 59, Ch. 3.
- [5] F. Abasalizadeh, S. V. Moghaddam, E. Alizadeh, E. Akbari, E. Kashani, S. M. B. Fazljou, M. Torbati, A. Akbarzadeh, *J. Biol. Eng.* **2020**, *14*, 8.
- [6] A. C. Hernández-González, L. Téllez-Jurado, L. M. Rodríguez-Lorenzo, *Carbohydr. Polym.* **2020**, *229*, 115514.
- [7] M. Farokhi, F. J. Shariatzadeh, A. Solouk, H. Mirzadeh, *Int. J. Polym. Mater. Polym. Biomater.* **2019**, *69*, 230.
- [8] B. H. A. Rehm, S., *Appl. Microbiol. Biotechnol.* **1997**, *48*, 281.
- [9] J. Sun, H. Tan, *Materials* **2013**, *6*, 1285.
- [10] H. Zhang, J. Cheng, Q. Ao, *Mar. Drugs* **2021**, *19*, 264.
- [11] G. T. Grant, E. R. Morris, D. A. Rees, P. J. Smith, D. Thom, *FEBS Lett.* **1973**, *32*, 195.
- [12] M. George, T. E. Abraham, *J. Control. Release* **2006**, *114*, 1.
- [13] Y. Fu, W. J. Kao, *Expert Opin. Drug Deliv.* **2010**, *7*, 429.
- [14] S. G. Reddy, *Alginates—A Seaweed product: Its Properties and Applications*, IntechOpen Book Series, London **2021**.
- [15] S. Singh, J. Dodt, P. Volkers, E. Hethershaw, H. Philippou, V. Ivaskevicius, D. Imhof, J. Oldenburg, A. Biswas, *Sci. Rep.* **2019**, *9*, 11324.
- [16] F. Fan, S. Saha, D. Hanjaya-Putra, *Front. Bioeng. Biotechnol.* **2021**, *9*, 718337.
- [17] K. Ino, M. T. Fukuda, K. Hiramoto, N. Taira, Y. Nashimoto, H. Shiku, *J. Biosci. Bioeng.* **2020**, *130*, 539.
- [18] A. Ahmed, G. Getti, J. Boateng, *Drug Deliv. Transl. Res.* **2018**, *8*, 1751.
- [19] H. Ahmed, B. T. Stokke, *Lab Chip* **2021**, *11*, 2232.
- [20] S. S. Waje, M. W. Meshram, V. Chaudhary, R. Pandey, P. A. Mahanawar, B. N. Thorat, *Braz. J. Chem. Eng.* **2005**, *22*, 209.
- [21] N. Wang, G. Adams, L. Buttery, F. H. Falcone, S. Stolnik, *J. Biotechnol.* **2009**, *144*, 304.
- [22] H. Zimmermann, F. Wählich, C. Baier, N. Westhoff, R. Reuss, D. Zimmermann, M. Behringer, F. Ehrhart, A. Katsen-Globa, C. Giese, U. Marx, V. L. Sukhorukov, J. A. Vásquez, P. Akob, S. G. Shirley, U. Zimmermann, *Biomaterials* **2006**, *28*, 1327.
- [23] R. H. Li, D. H. Altreuter, F. T. Gentile, *Biotechnol. Bioeng.* **1996**, *50*, 365.
- [24] A. Jejurikar, G. Lawrie, D. Martin, L. Grøndahl, *Biomed. Mater.* **2011**, *6*, 025010.
- [25] J. Schmid, B. Burkhard, W. Yeo, R. Z. Zhang, *Anal. Bioanal. Chem.* **2008**, *391*, 1899.
- [26] Y. Suzuki, Y. Nishimura, M. Tanihara, K. Suzuki, T. Nakamura, Y. Shimizu, Y. Yamawaki, Y. Kakimaru, *J. Biomed. Mater. Res.* **1998** Feb, *39*, 317.
- [27] S. E. Barnett, S. J. Varley, *Ann. R. Coll. Surg. Engl.* **1987**, *69*, 153.
- [28] P. A. Kallenberger, M. Fröba, *Commun. Chem.* **2018**, *1*, 28.
- [29] J. Cai, X. Chen, X. Wang, Y. Tan, D. Ye, Y. Jia, P. Liu, H. Yu, *RSC Adv.* **2018**, *8*, 39463.
- [30] K. Bialik-Wąs, E. Rólicka, D. Malina, *Molecules* **2021**, *26*, 2381.
- [31] F. Cuomo, M. Cofelice, F. Lopez, *Polymers (Basel)* **2019**, *11*, 259.
- [32] H. Daemi, M. Barikani, *Sci. Iran.* **2012**, *19*, 2023.
- [33] K. Y. Lee, D. J. Mooney, *Prog. Polym. Sci.* **2012**, *37*, 106.
- [34] S. K. Papageorgiou, E. P. Kouvelos, E. P. Favvas, A. A. Sapalidis, G. E. Romanos, F. K. Katsaros, *Carbohydr. Res.* **2010**, *345*, 469.
- [35] Y. L. Patel, P. Sher, A. P. Pawar, *AAPS PharmSciTech* **2006**, *7*, 86.

- [36] S. R. Abulateefeh, M. O. Taha, *J. Microencapsul.* **2014**, *32*, 96.
- [37] H. M. Jensen, F. H. Larsen, S. B. Engelsen, in *Methods in Molecular Biology*, Vol. 1308 (Eds: D. B. Stengel, S. Connan), Springer, Berlin **2015**, p. 347.
- [38] C. K. Kuo, P. X. Ma, *Biomaterials* **2001**, *22*, 511.
- [39] Z. Belattmania, S. Kaidi, S. El Atouani, C. Katif, F. Bentiss, C. Jama, A. Reani, A. Reani, B. Sabour, V. Vasconcelos, *Molecules* **2020**, *25*, 4335.
- [40] A. S. Prasad, *Mol. Med.* **2008**, *14*, 353.
- [41] A. Aycicek, A. Koc, Y. Oymak, S. Selek, C. Kaya, B. Guzel, *J. Pediatr. Hematol. Oncol.* **2014**, *36*, 57.
- [42] A. M. P. Romani, *Int. J. Hypertens.* **2018**, *2018*, 9013721.

SUPPORTING INFORMATION

Additional supporting information can be found online in the Supporting Information section at the end of this article.

How to cite this article: E. Man, A. Oluwasanmi, D. A. Lamprou, K. Goudie, J. Liggat, C. Hoskins, *J. Appl. Polym. Sci.* **2022**, e52941. <https://doi.org/10.1002/app.52941>